Triangular laser-induced submicron textures for functionalising stainless steel surfaces

Romano, Jean-Michel; Garcia Giron, Antonio; Penchev, Pavel; Dimov, Stefan

DOI:
10.1016/j.apsusc.2018.01.086

Document Version
Peer reviewed version

Citation for published version (Harvard):
Romano, J-M, Garcia Giron, A, Penchev, P & Dimov, S 2018, 'Triangular laser-induced submicron textures for functionalising stainless steel surfaces', *Applied Surface Science*, vol. 440, pp. 162-169. https://doi.org/10.1016/j.apsusc.2018.01.086

Triangular laser-induced submicron textures for functionalising stainless steel surfaces

Jean-Michel Romano *, Antonio Garcia Giron, Pavel Penchev, Stefan Dimov

Department of Mechanical Engineering, School of Engineering, University of Birmingham, Birmingham B15 2TT, United Kingdom

* J.Romano@bham.ac.uk

ABSTRACT

Processing technologies that engineer surfaces with sub-micron topographies are of a growing interest to a range of optical, hydrophobic and microbiological applications. One of the promising technologies for creating such topographies employs ultra-short laser pulses to produce laser-induced periodic surface structures (LIPSS) that often result in non-regular, quasi-periodic nanoripples and nanopillars. In this research near infrared ultra-short pulses of 310 fs with a circular polarisation was used to texture ferritic stainless steel workpieces. A single-step process was designed to generate low spatial frequency LIPSS (LSFL) over relatively large areas. Apart from highly regular and homogeneous parallel lines with approximately 900 nm periodicity extraordinarily uniform triangular-LSFL in hexagonal arrangements was created. The generation of such LSFL was found to be highly repeatable but very sensitive to the used laser processing settings. Therefore, the sensitivity of triangular-LSFL formation to the used laser processing settings, i.e. pulse to pulse distance, pulse fluence and focal plane offsets, were investigated in regard to the resulting morphologies and functional properties, i.e. structural colors and super-hydrophobicity. Finally, the capability of this technology for producing uniform triangular-shaped LSFL on relatively large surface areas of stainless steel plates was studied.

Keywords

LIPSS, femtosecond laser, large area, uniformity, wettability, light scattering

1 INTRODUCTION

The interest and research activities in the field of laser-induced periodic surface structures (LIPSS) have been growing in recent years due to their promising applications for surface functionalisation. In particular, such surface engineering technology has been used for decorative purposes [1], anti-counterfeiting [2] and improved solar cell efficiency [3] due to the resulting structural coloring, broadband light absorption, antireflection and blackening effects. In addition, surfaces processed in this way exhibit a superhydrophobic behaviour that finds applications in self-cleaning [4] and anti-icing [5]. Another area is biomedical, i.e. dental and orthopaedic implants, where LIPSS textured surfaces have been used to influence biocompatibility [6], cell proliferation [7] and also bacterial adhesion and biofilm formation [8,9]. Furthermore, LIPSS texturing of hard coatings has also been investigated for tribological applications [10].

These applications can require surface topographies with dimensions in the sub-micron range. Therefore, ultra-short laser pulses are used to generate a plethora of low spatial frequency LIPSS (LSFL), such as nanoroughness, nanopillars and nanogratings, with periodicities much lower than the laser spot size. There are many factors affecting their generation such as irradiated material and laser wavelength [11], beam polarisation [12], fluence per pulse and number of pulse [13], but also the irradiation environment [14] and irradiation angle [15]. LSFL are usually orientated perpendicular to the incident linear polarisation and have a spatial periodicity close to the laser wavelength [11]. In the case of circular polarisation, several cases can be observed: wavy ripple-like LSFL generated at 45° orientation [12,16]. With the increase of the total energy dose per unit area, referred to as accumulated fluence,

early-stage LIPSS undergo a sharp change in periodicity and uniformity [17]. When both peak fluence and accumulated fluence increase, more complex, hierarchical LIPSS referred to as micro-bumps can be obtained [18]. Bumpy surfaces are shown to be a consequence of heat accumulation at high average power and repetition rates [19].

Such complex LIPSS can be generated with linear polarised femtosecond laser pulses by tailoring a compound mix of LIPSS in the sub-micron range [20]. Furthermore multi-scale topographies can be obtained by using a pre-processed surface [21]. The fabrication of rhombic-shaped LIPSS can be achieved using promising single-step laser processes using a dynamic rotation of polarisation [12] or a cylindrical vector beams generated with a radial polarisation converter [22]. Another approach is the two-step processing employing a train of pulses or multiple passes with varying relative orientation of the scans in regard to the polarisation direction that lead to square- or diamond-shaped LIPSS. Superimposition of LIPSS can occur with significantly less fluence per pulse than that used in the initial pulses [9,23,24].

The texturing of larger surfaces with such self-organised quasi-periodic nanofeatures is essential to broaden the use of this technology for surface functionalisation in a number of promising application areas. Such large-area texturing has been investigated by employing different processing strategies, e.g. the use of moving discrete spot laser irradiation to merge LIPSS [25,26] or through pulse overlapping [18,27–30]. High repetition rates combined with high scanning speed, in the order of MHz and m/s respectively, has also been shown to enable area processing with sufficient pulse fluence and pulse overlap to generate uniform LIPSS in one pass; the uniformity being then obtained by optimising the distance between scanned lines [29]. However, potential local non-uniformities of LIPSS are known to occur as

a result of preceding polishing step [28,31], grain boundaries [32] and surface defects [28]. Uniformity of LIPSS generation can potentially be improved using pre-processed gratings [21,33].

In this paper, the LIPSS generation on stainless steel plates in ambient air is presented. A single-step femtosecond laser process (one pass) is investigated using high scanning speed and pulse frequency, up to 1 m/s and 500 kHz, respectively, to enable high-throughput processing. The generation of uniform large-area LIPSS with Gaussian intensity laser beam is studied. In addition to wavy and relatively disorganised LSFL reported in literature [12,16,22], this research presents a single-step texturing with highly regular linear-LSFL and triangular-like LSFL in hexagonal arrangements employing a conventional beam delivery set-up with circular polarisation. The functional properties of processed surfaces in terms of light scattering and wettability are also investigated together with process robustness, in particular the sensitivity of the texturing process to variations in the focal position.

2 MATERIAL AND METHODS

Commercially available X6Cr17 ferritic stainless steel plates with 0.7 mm thickness and average roughness of $R_a = 35$ nm are used in this research.

The texturing was performed using a femtosecond laser source (Satsuma from Amplitude Systemes) with the following technical characteristics, a central wavelength, λ, of 1032 nm, 310 fs pulse duration, a maximum pulse repetition rate of 500 kHz and 5 W average power. The beam line incorporates a beam expander and a quarter waveplate to convert the s-type linear polarisation of the laser source into a circular one. A galvo scan head (RhoThor RTA) equipped with a 100-mm focal length telecentric lens is used to deflect the laser beam over the surface. The spot diameter $2\omega_0$ at $1/e^2$ is 30 μm.

Initially, the field textured were limited to 3 x 3 mm^2 in order to study the LSFL generation. Then, larger areas up to 40 x 40 mm^2 were processed without stitching in order to investigate the surface wettability and optical properties. The theoretical depth of focus is 1.1 mm, in particular twice the Rayleigh length $z_R = \pi {\omega_0}^2/(\lambda M^2)$, where M^2 is better than 1.2 for the used laser source.

The samples were positioned normal to the incident beam and fixed onto a 5-axis motorised stage that allows three linear and two angular movements. All texturing trials were performed in atmospheric conditions.

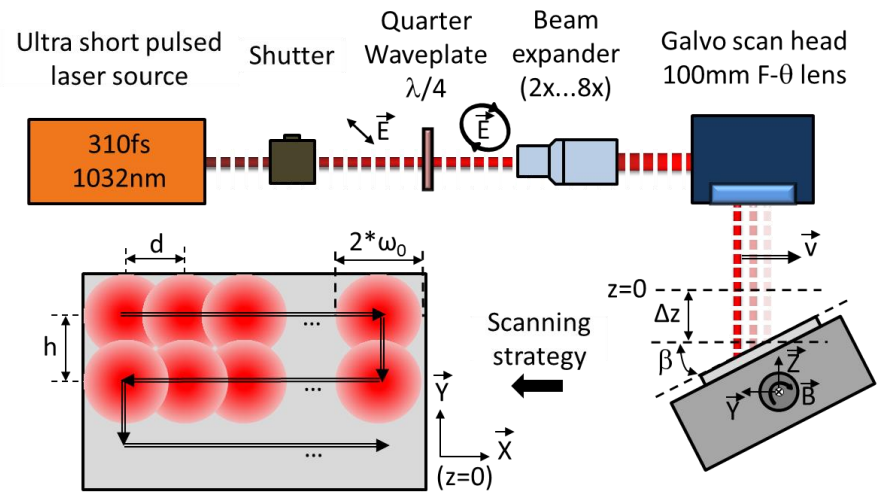

Figure 1: Beam line components and scanning strategy.

The textured areas were processed line by line, using a bidirectional raster scanning strategy. The distance between scan lines is defined as hatch distance, h, ranging from 1 μm to 10 μm. The scanning is executed with a variable velocity, v, from 100 mm/s to 1500 mm/s and pulse repetition rates, f, from 50 kHz to 500 kHz. The distance between two consecutive spot centres is therefore given by:

$$d = v/f \qquad (1)$$

The effective number of pulses per beam spot is calculated by $2\omega_0/d$ while the effective number of pulses per unit area, N, is:

$$N = \frac{\pi {\omega_0}^2}{dh} \qquad (2)$$

The overlap, O, between two consecutive circular pulses can be approximated by the geometrical equation [34]:

$$O = \frac{1}{\pi\omega_0}\left\{2\omega_0 \cos^{-1}\left(\frac{d}{2\omega_0}\right) - d\sqrt{1-\frac{d}{2\omega_0}^2}\right\} \qquad (3)$$

Surfaces were textured with varying average power, P, and pulse repetition rates, f, and thus the pulse fluence could be calculated as $\varphi_0 = P/(\pi\omega_0{}^2 f)$. The effective accumulated fluence per unit area, φ, can then be approximated as follows:

$$\varphi = N\varphi_0 = \frac{P}{fdh} \qquad (4)$$

The sub-micron textures of processed surfaces were analysed using a tabletop scanning electron microscope (SEM) (Hitachi TEM3030Plus).

The wetting properties were characterised using the sessile droplet method employing Attension Theta Optical Tensiometer. In particular, Milli-Q waterdrops of 6 μl were dispensed under atmospheric conditions onto the textured surfaces and the average value of the static contact angle (CA) was obtained after stabilisation. No chemical product was used to clean the laser processed samples and any debris were removed by using compressed air.

3 RESULTS AND DISCUSSION

3.1 PROCESS OPTIMISATION FOR UNIFORM LSFL

The first part of the research reported in this paper was focused on optimising a single pass laser process for texturing large areas with low spatial frequency LIPSS (LSFL) that are referred to as LIPSS from this point on in the paper. As typically these types of self-organised structures occur below and around the ablation threshold, the first objective was to find the LIPSS threshold. This was achieved by adjusting the pulse energy while keeping the other processing parameters constant, i.e. scanning speed of 500 mm/s and pulse repetition rate of 250 kHz. The scanning strategy to achieve a high overlap was initially used to minimise the rim effect of the Gaussian intensity beam as illustrated in [35]. In particular, the pulse to pulse distance was the same over the surface (d = h = 2 μm, N = 177, O = 92%) and the LIPSS threshold was found to be at φ_0 = 28 mJ/cm^2. By increasing fluence and varying the scanning speed various types of surface structures were produced. Typical micrographs illustrating the evolution of LIPSS are shown in Figure 2. The first stage of LIPSS induced by the circularly polarised beam were observed at low levels of accumulated fluence, i.e. around 5 J/cm^2 (Fig 2a) corresponding to 0.65 μJ pulses at 1500 mm/s. The periodicity, Λ, given by the 2D-FFT laid below the laser wavelength, i.e. at around 800 to 900 nm. The quasi circular Fourier Transform confirmed the LIPSS morphology with no specific periodic direction.

By varying pulse energy and scanning speed, and hence the pulse-to-pulse distance, intermediate stages of LIPSS were observed progressively where the ripples were self-organised in a very consistent and uniform manner (Fig 2c). In particular, the resulting LIPSS

morphology looked like triangles where the ripples were divided in triangular-like sub-sections. A long-range hexagonal arrangement is indicated by the 2D-FFT that depicts distinctly 3 directions of periodicity with an angular shift of around 60°.

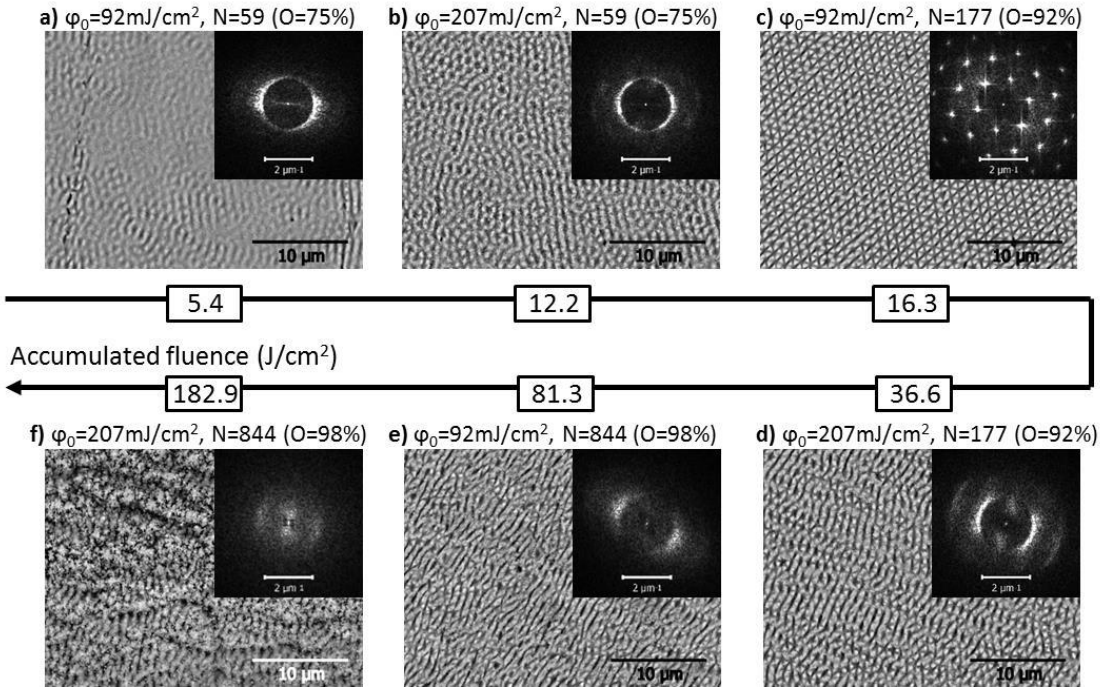

Figure 2: The LIPSS evolution with the increase of accumulated fluence with 250 kHz and 2 μm hatching settings.

The increase of accumulated fluence at the early stages led to the formation of LIPSS with more defined ripples with the same range of periodicity (Fig 2a-b). However, the highly uniform triangular-LIPSS are continuously erased at the later stages of their evolution. In particular, the merger of triangular-LIPSS into ripples was observed that led to a mix of triangles and ripples. 2D-FFTs of LIPSS shown in Figures 2d-e indicate a continuous alignment into ripple-like LIPSS. At higher accumulated fluence, sub-micron roughness can be observed on ripples (Fig 2e) until covering all LIPSS (Fig 2f).

By varying the fluence per pulse and scanning speed while keeping the other parameters constant, a cartography of the LIPSS morphologies was drawn as shown in Figure 3. The processing window for generating uniform triangular-LIPSS was identified, especially pulse fluence from 71 to 144 mJ/cm^2 and 118 to 353 pulses were used to achieve an accumulated fluence in the range from 10.8 to 25.2 J/cm^2.

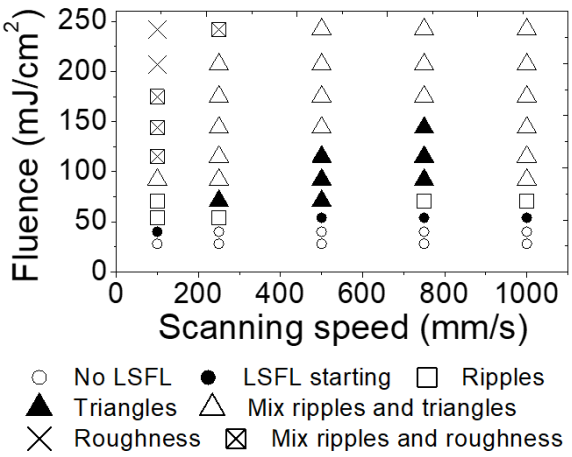

Figure 3: LIPSS morphologies as a function of scanning speed and pulse fluence with 250 kHz and 2 μm hatching settings.

A thorough analysis of the LIPSS periodicity and orientation was carried out by varying the pulse fluence while frequency, scanning speed and hatching distance were fixed at 250 kHz, 500 mm/s and 2 μm, respectively. The LIPSS periodicities vary between 0.84 and 0.98 μm but remain below 1.03μm, the laser wavelength, as depicted in Figure 4a. At φ_0 = 54 mJ/cm^2, the ripple-like LIPSS have a periodicity (Λ) of 0.85 μm and an orientation (α) of -15°. With pulse fluence in the range from 71 to 91 mJ/cm^2 triangular-LIPSS are generated with multi-directional periodicities, ranging from 0.90 to 0.98 μm. Wavy ripple-like LIPSS with 0.85

μm periodicity are observed at higher pulse fluence. Variations of pulse fluence seem to influence the triangular-LIPSS formation. In particular, when φ_0 increased from 71 to 92 mJ/cm^2, the overall hexagonal orientation (α_1, α_2, α_3) underwent a general shift of 6° clockwise and the third periodicity Λ_3 decreased from 0.98 to 0.93 μm. Figure 4b provides more details about the measurements of Λ and α in the carried out FFT analysis. The orientations, α, of the triangular-LIPSS showed a surprising consistency compared to the other LIPSS morphologies, especially the α spread was from +/- 1° to 4° compared to +/- 17° and +/-38° at 54 and 207 mJ/cm^2, respectively.

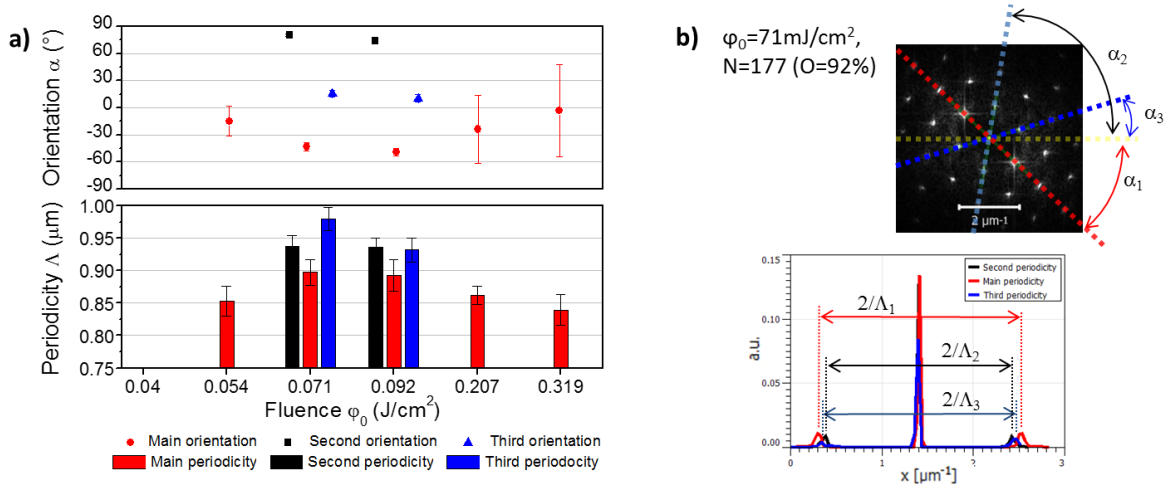

Figure 4: Evolution of LIPSS periodicity and orientation with the pulse fluence with 250 kHz, 500 mm/s and 2 μm hatch (a). Example of 2D-FFT analysis in the case of φ_0 = 71 mJ/cm^2 (b).

The second part of the research investigated the influence of other processing parameters. In particular, experiments were performed for each parameter separately while the average power and the scanning speed were kept constant in order to find the optimum process settings and also to study their effects on LIPSS texturing.

The influence of hatch distance when varied in the range from between 1 to 20 μm was investigated. The surface was not entirely covered with LIPSS when hatching of 10 μm and higher were used and only early stage LIPSS with periodicity of 0.94 μm at -17° appeared in the centre of the laser track. At the same time 2 distinct ripple directions were observed when the hatch distance was decreased to bring the LIPSS textured laser track together, and a periodicity of 0.92 μm at -53° was mixed with the periodicity resulting at higher spacing (Fig 5a). At 3 μm hatching, 3 more periodicities were added to the 2 earlier ones, i.e. 0.98μm/6°, 1.50μm/57° and 0.97μm/71°, and LIPSS with triangular shapes began to appear but without a clear homogeneity (Fig 5b). At h = 2 μm (0.87μm/-47°, 0.97μm/11°, 0.93μm/77°) the triangular-LIPSS were very uniform as stated earlier while a further decrease of hatch distance led to a disappearance of uniformity and only the main periodicity at -42° remained (Fig 5c). Based on this empirical analysis a hypothesis could be drawn on the triangular-LIPSS formation mechanism, in particular the triangles would appear in the transition phase between early linear-LIPSS oriented at -17° and later LIPSS at -42°, where sufficient accumulated fluence leads to a separation of the ripple-like LIPSS into triangles.

The variation of pulse repetition rates, i.e. the use of 10, 50, 100, 250 and 500 kHz, didn't allow the triangular-LIPSS to be retained and this could be attributed to some significant changes both in pulse energy and pulse-to-pulse distance. In addition, no surface damage was detected at 10 kHz while early-stage ripple-like LIPSS of single periodicity of 0.92 μm at -17° were observed at 50 kHz (Fig 5d). The process settings at f = 100 kHz (N=71, φ_0 = 68 mJ/cm^2) resulted in highly uniform and regular linear-LIPSS with periodicity of 0.90 μm and orientation at 40° (Fig 5e). While process settings in Figure 2b are similar to those in Figure 5e, φ of 12.2 and 12.6 J/cm^2, respectively, LIPSS morphologies differs, especially resulting

in uneven ripples and aligned ripples with a spatial periodicity of Λ = 0.90 μm, correspondingly. This effect may be due to different time delays in delivering trains of pulses [36] and to different pulse-to-pulse distance [2]. The LIPSS in Figure 5e was used to compare the surface functionalities of linear- and triangular-LIPSS in this research. A further increase of pulse repetition rate led to the loss of straight lines uniformity and the generation of ripple-like LIPSS (Fig 5f).

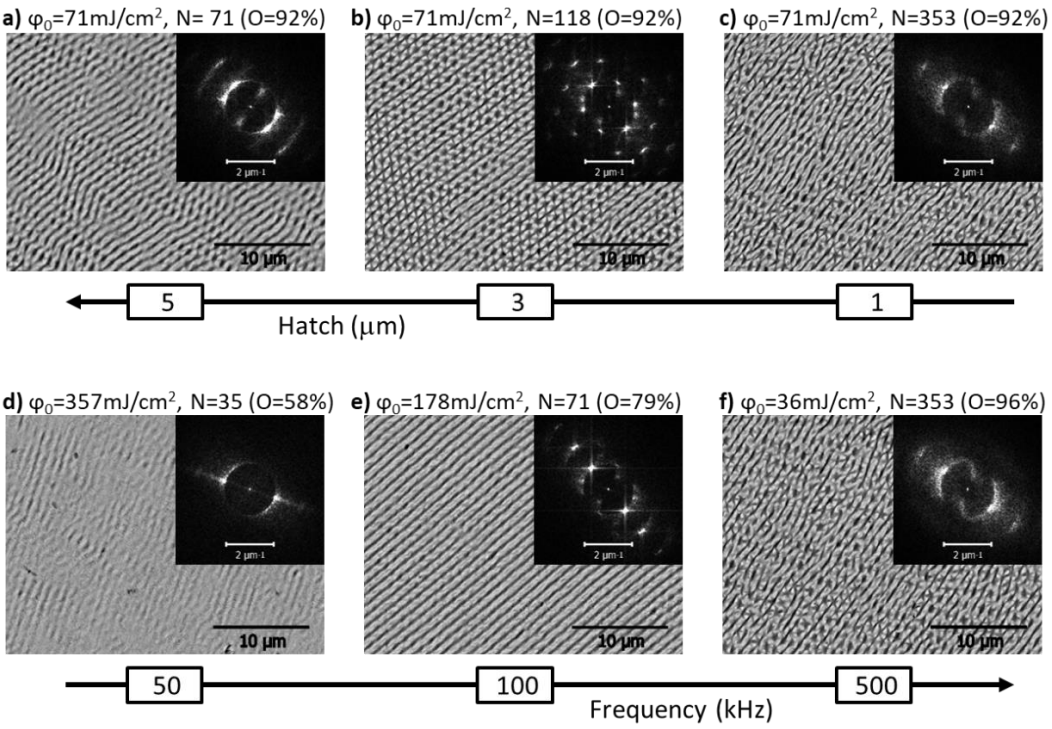

Figure 5: The LIPSS evolution: (a-c) with the decrease of hatching distance with fixed pulse frequency of 250 kHz, scanning speed of 500 mm/s and pulse fluence of 71 mJ/cm^2; and (d-f) with the increase of pulse repetition rate at fixed φ of 12.6 J/cm^2.

The influence of scan repetitions over the processed area was analysed by increasing them from 1 to 10 while using the following process settings: φ_0 = 92 mJ/cm^2 and N = 177. A clearly defined hexagonal 2D-FFT signifying a uniform triangular arrangement of LIPSS was obtained after the first scan only and then disappeared after the second one (Fig 6a-c). In

particular, the main periodicity decreased from $\Lambda \sim 0.87$ to 0.74 μm while the orientation shifted from $\alpha \sim -46°$ to $\sim -26°$. An additional test was performed at a lower fluence per pulse (φ_0 = 54 mJ/cm^2), just above the LIPSS threshold, where LIPSS appeared only on some very localised surface defects but it was not possible to texture the whole area that was scanned (Fig 6d). The increase in scan numbers led to ripple-like LIPSS texturing, with a decrease in the periodicity without changing significantly the periodicity orientation (Fig 6e-f). Figures 6a and 6e depict that the use of similar accumulated fluence (respectively 16 and 19 J/cm^2) but with different pulse fluence and number of pulses can result in different LIPSS, i.e. triangular- and ripple-like LIPSS, respectively.

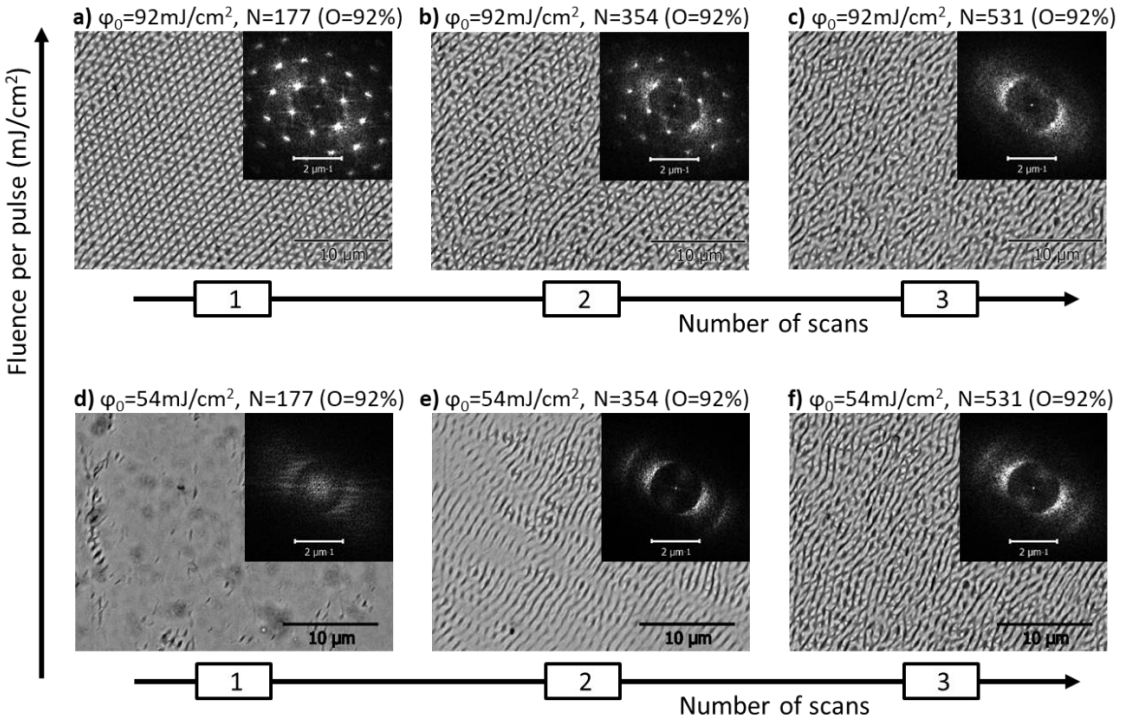

Figure 6: The LIPSS evolution with the scan number increase: (a-c) φ_0 of 92 mJ/cm^2; (d-f) φ_0 of 54 mJ/cm^2.

3.2 FORMATION OF LIPSS IN HEXAGONAL ARRANGEMENTS

There is still no consensus on the mechanism of quasi-periodic ripples-like LIPSS formation. LIPSS induced with linear polarisation has been widely considered to result from the interference of incident laser beams with surface-scattered waves generated by rough surfaces [37]. The excitation and resonance of surface plasmon polaritons [38] might also play a significant role in the LIPSS generation.

Hexagonal self-organisation of nanoparticles was observed by irradiating TiO_2 thin films and silver nanoparticles with green CW circularly polarised light [39]. It is suggested that the mesoporous characteristic of TiO_2 facilitates the movement of nanoparticles. The migration of nanoparticles may be the result of the same phenomena as that observed in this research. In particular, the scanning of substrates with circularly polarised laser beams can generate hexagonal-shaped arrangements in specific conditions. The symmetries induced by such hexagonal arrangements may then lead to triangular-shaped LIPSS formation.

As LIPSS are evolving with the increase of pulse numbers, simulation of the electric field distribution after linearly polarised irradiation onto submicron grooves, representing early stage linear-LIPSS, was investigated by several researchers [20,40]. Ji et al used a linearly polarised femtosecond laser to fabricate a complex mix of cross-periodic LIPSS on Si substrates. It was experimentally demonstrated that the first pulses generated typical linear-LIPSS but with the increase of pulse numbers a perpendicular sub-division of LIPSS occurred while the periodicity was similar. The simulation the electric field distribution after irradiation of linear-LIPSS suggested that the phenomena could be attributed to local maxima in the electric field distribution inside their grooves [20]. However, Hou et al reported a

parallel subdivision of LIPSS that decreased the LIPSS periodicity by half. This experimental observation was confirmed by referring to the surface-scattered wave theory and simulating the electric filed distribution after irradiation and reflection from linear-LIPSS grooves [40]. Similar to what was observed and simulated with linearly polarised irradiation, circular polarisation could lead to a more complex sub-division of LIPSS. Thus, a simulation of circularly polarised beam irradiation onto early-stage LIPSS may provide some insights into the complex maxima patterns of the electric field distribution and potentially to explain the hexagonal arrangement of triangular-LIPSS.

Another aspect to consider in regard to the triangular-LIPSS formation that can affect the process repeatability is the potential misalignment of the quarter waveplate. As reported by Varlamova et al, a slight misalignment can lead to elliptical polarisation instead of a circular one and this may have a significant impact on the LIPSS generation and may lead to different LIPSS morphologies [41]. In this work, a slight shift of the linear-LIPSS arrangements was observed during the early-stage LIPSS generation and also in the evolution of the triangular-LIPSS. However, the mechanism driving the LIPSS hexagonal arrangement has to be investigated further in both empirical and theoretical studies.

3.3 SURFACE FUNCTIONALITY

Surface functionalities of two LIPSS types were analysed in this research, i.e. triangular- and linear-like LIPSS depicted in Figures 3b and 5e, respectively. The wettability of a representative 16mm^2 area was measured after stabilisation of the water drop on the textured surface. Following the laser texturing, the samples exhibited superhydrophilic behaviour, which lasted approximately 1-2 days while the samples were store in ambient conditions, and

then they became gradually superhydrophobic and reached a steady state after one week. Starting with a static contact angle of 96.0° ± 3.5° prior to laser texturing, values of 145.7° ± 0.8° and 157.1° ± 1.6° were achieved for linear- and triangular-LIPSS, respectively (Figures 7a-b at Δz=0). The time dependent wettability of femtosecond LIPSS was reported by research groups [22,27,42,43], however the phenomenon remains largely not fully understood. Modification of surface chemistry together with activation and adsorption of hydrocarbon molecules by the resulting organic layer could explain this phenomenon [27,42,44]. The storage condition of the laser-textured samples also plays an important role in the aging process [34].

While both LIPSS morphologies had a similar hydrophobic behaviour, the hexagonal arrangement of triangular LIPSS may benefit from its more complex morphologies, the multiple axis of symmetry and well-defined uniformity in different ways. The wetting behaviour of ripple-like LIPSS have been reported to show an anisotropic behaviour, where the water drop tends to elongate itself in the LIPSS direction [45]. While no water drop elongation has been observed in the present work, the three axes of symmetry of the triangular-LIPSS may minimise any anisotropic effect and also may lead to a multi-directional self-cleaning functionalisation.

The optical properties of both LIPSS morphologies were investigated, too, using a single white LED light source. The light scattering was observed for different combinations of light incident and observation angles. While such structural colors are widely reported to be dependent on the orientation of linear-LIPSS or on more randomly distributed ripples-like LIPSS [1,2] or rhombic-shaped LIPSS [22], the multiple axes of symmetry of the triangular-LIPSS may exhibit structural colors in multiple directions and further research is currently

ongoing to investigate potential applications of this technology in decoration and anti-counterfeiting.

3.4 INFLUENCE OF FOCAL POSITION ON SURFACE FUNCTIONALITY

Large surfaces may have localised defects or slight variation in planarity that may influence greatly early stage LIPSS formation, and thus to lead to ripples instead of uniform lines or triangles. Changes in LIPSS generation when processing out of focus or with incident beam that was not normal to the processed surface were widely reported by research groups, especially in term of their homogeneity, morphology and periodicity [15,43].

The effect of focal position variations on LIPSS formation was investigated on two LIPSS morphologies studied in this research (the triangular- and linear-LIPSS shown in Figures 3b and 5e). In particular, out of focus texturing was performed with offsets of 50, 100, 150, 200, 250, 300, 500, 750 and 1000 μm in both positive and negative direction from the focal point. The resulting surface functionalities are depicted in Figures 7a-b.

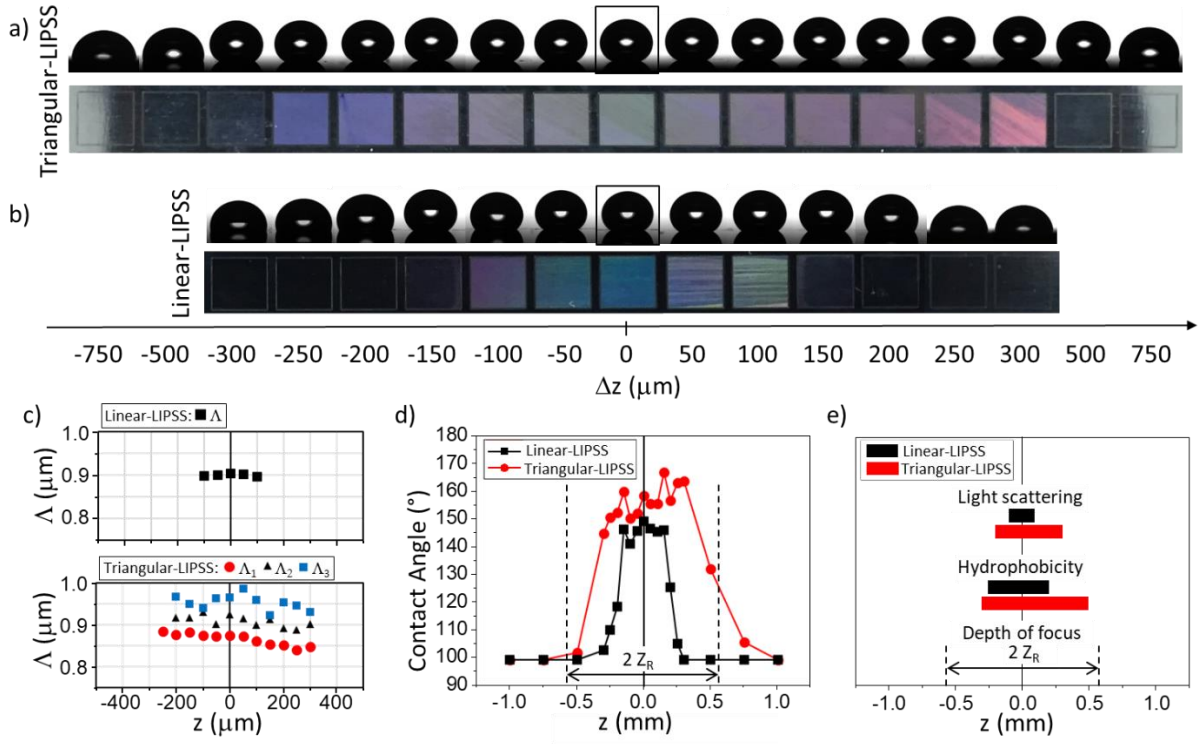

Figure 7: The influence of focal plane offsets on (a) triangular-LIPSS and (b) linear-LIPSS and their evolution in (c) LIPSS periodicity and (d-e) surface functionalities.

When off focus processing is carried out, the beam size, pulse overlap and pulse fluence are inherently modified. However, the main periodicities of LIPSS processed off focus remain relatively constant for both the linear-LIPSS (Λ = 0.90 μm) and the triangular LIPSS (Λ_1 = 0.84 to 0.88 μm) as depicted in Figure 7c. Non-uniform LIPSS were observed when Δz was higher than 200 and 500 μm, for linear- and triangular-LIPSS, respectively. It is worth mentioning that triangular-LIPSS were not generated at z = -250 μm and only non-uniform ripples were observed but the surface functionality was not affected.

To assess the depth of focus for the structural coloring, a binary state was considered by visually observing the sample at different combination of lighting and observation angles. Contact angles are measured after surface stabilisation like described in Section 3.3 and

presented in Figure 7d. The laser processed surface is considered functionalised when contact angle changes are higher than ± 10% of the reference value for unprocessed surfaces.

The results in Figure 7e show that if the offset is within the theoretical depth of focus (estimated at 1.1 mm in Section 2), the surface properties cannot be maintained for both LIPSS types. No structural coloring was observed when Δz was higher than 200 and 550 μm, for the linear- and triangular-LIPSS, respectively. The surface wettability was the same ~~as~~ that on unprocessed samples when Δz was higher than 450 and 800 μm, for linear- and triangular-LIPSS, respectively. Hence, the depth of focus associated with the hydrophobic property is higher than that for structural coloring.

4 CONCLUSION

The successful generation of uniform Laser-Induced Periodic Surface Structures (LIPSS) was demonstrated on ferritic stainless steel employing a one-step processing approach in air with a circularly polarised femtosecond laser source. Low Spatial Frequency LIPSS (LSFL) were produced exhibiting highly uniform distinct triangular-shapes in hexagonal arrangement over relatively large surface areas. A texturing approach was designed by investigating the effects of pulse fluence and both scanning speed and repetition rates. In addition, the sensitivity of this approach to off focus processing in generating LIPSS was studied. The triangular-LIPSS were demonstrated for a narrow, however highly repeatable laser processing window at a rate of approximately 1 mm^2/s. Such LIPSS exhibited light scattering and superhydrophobic properties, with contact angles as high as 157° after surface stabilisation through storage at ambient conditions. Using constant processing parameters and an optimised scanning strategy, the depth of focus associated with investigated functional properties, i.e. structural colors and hydrophobicity, was determined. The approach studied in this research represents a new concept in large-area ultrafast laser structuring, where the accumulated fluence was a key factor in achieving a uniform texturing and thus functionalisation of metallic plates with some planarity deviations.

ACKNOWLEDGMENTS

The research reported in this paper was carried out within the framework of European Commission H2020 ITN programme “European ESRs Network on Short Pulsed Laser Micro/Nanostructuring of Surfaces for Improved Functional Applications” (Laser4Fun) under the Marie Skłodowska-Curie grant agreement No. 675063 (www.laser4fun.eu). In addition, the work was supported by two other H2020 FoF programmes, i.e. the projects on “Modular laser based additive manufacturing platform for large scale industrial applications” (MAESTRO) and “High-Impact Injection Moulding Platform for mass-production of 3D and/or large micro-structured surfaces with Antimicrobial, Self-cleaning, Anti-scratch, Anti-squeak and Aesthetic functionalities” (HIMALAIA). The authors would like also to acknowledge the support and assistance of Behnam Dashtbozorg and Shaojun Qi from the School of Metallurgy and Materials at the University of Birmingham, in the sample preparation and the SEM characterisation.

REFERENCES

[1] B. Dusser, Z. Sagan, H. Soder, N. Faure, J.P. Colombier, M. Jourlin, E. Audouard, Controlled nanostructrures formation by ultra fast laser pulses for color marking, Opt. Express. 18 (2010) 2913–2924. doi:10.1364/OE.18.002913.

[2] J. Yao, C. Zhang, H. Liu, Q. Dai, L. Wu, S. Lan, A.V. Gopal, V.A. Trofimov, T.M. Lysak, Selective appearance of several laser-induced periodic surface structure patterns on a metal surface using structural colors produced by femtosecond laser pulses, Appl. Surf. Sci. 258 (2012) 7625–7632. doi:10.1016/j.apsusc.2012.04.105.

[3] B.K. Nayak, V.V. Iyengar, M.C. Gupta, Efficient light trapping in silicon solar cells by ultrafast-laser-induced self-assembled micro/nano structures, Prog. Photovolt. Res. Appl. 19 (2011) 631–639. doi:10.1002/pip.1067.

[4] A.Y. Vorobyev, C. Guo, Multifunctional surfaces produced by femtosecond laser pulses, J. Appl. Phys. 117 (2015) 033103. doi:10.1063/1.4905616.

[5] A.-M. Kietzig, M.N. Mirvakili, S. Kamalb, P. Englezos, S.G. Hatzikiriakos, Nanopatterned Metallic Surfaces: Their Wettability and Impact on Ice Friction, J. Adhes. Sci. Technol. 25 (2011) 1293–1303. doi:10.1163/016942411X555872.

[6] C. Liang, H. Wang, J. Yang, B. Li, Y. Yang, H. Li, Biocompatibility of the micro-patterned NiTi surface produced by femtosecond laser, Appl. Surf. Sci. 261 (2012) 337–342. doi:10.1016/j.apsusc.2012.08.011.

[7] S. Schlie, E. Fadeeva, A. Koroleva, B.N. Chichkov, Laser-engineered topography: correlation between structure dimensions and cell control, J. Mater. Sci. Mater. Med. Lond. 23 (2012) 2813–9. doi:10.1007/s10856-012-4737-9.

[8] E. Fadeeva, V.K. Truong, M. Stiesch, B.N. Chichkov, R.J. Crawford, J. Wang, E.P. Ivanova, Bacterial Retention on Superhydrophobic Titanium Surfaces Fabricated by Femtosecond Laser Ablation, Langmuir. 27 (2011) 3012–3019. doi:10.1021/la104607g.

[9] A. Cunha, A.-M. Elie, L. Plawinski, A.P. Serro, A.M. Botelho do Rego, A. Almeida, M.C. Urdaci, M.-C. Durrieu, R. Vilar, Femtosecond laser surface texturing of titanium as a method to reduce the adhesion of Staphylococcus aureus and biofilm formation, Appl. Surf. Sci. 360, Part B (2016) 485–493. doi:10.1016/j.apsusc.2015.10.102.

[10] J. Bonse, S.V. Kirner, R. Koter, S. Pentzien, D. Spaltmann, J. Krüger, Femtosecond laser-induced periodic surface structures on titanium nitride coatings for tribological applications, Appl. Surf. Sci. 418, Part B (2017) 572–579. doi:10.1016/j.apsusc.2016.10.132.

[11] S. Bashir, M. Shahid Rafique, W. Husinsky, Femtosecond laser-induced subwavelength ripples on Al, Si, CaF2 and CR-39, Nucl. Instrum. Methods Phys. Res. Sect. B Beam Interact. Mater. At. 275 (2012) 1–6. doi:10.1016/j.nimb.2011.12.016.

[12] S. Graf, F.A. Muller, Polarisation-dependent generation of fs-laser induced periodic surface structures, Appl. Surf. Sci. 331 (2015) 150–155. doi:10.1016/j.apsusc.2015.01.056.

[13] K.M.T. Ahmmed, E.J.Y. Ling, P. Servio, A.-M. Kietzig, Introducing a new optimization tool for femtosecond laser-induced surface texturing on titanium, stainless steel, aluminum and copper, Opt. Lasers Eng. 66 (2015) 258–268. doi:10.1016/j.optlaseng.2014.09.017.

[14] L.S. Jiao, E.Y.K. Ng, H.Y. Zheng, Refining femtosecond laser induced periodical surface structures with liquid assist, Appl. Surf. Sci. 264 (2013) 52–55. doi:10.1016/j.apsusc.2012.09.101.

[15] J. Wang, C. Guo, Formation of extraordinarily uniform periodic structures on metals induced by femtosecond laser pulses, J. Appl. Phys. 100 (2006) 023511. doi:10.1063/1.2214464.
[16] O. Varlamova, J. Reif, S. Varlamov, M. Bestehorn, The laser polarization as control parameter in the formation of laser-induced periodic surface structures: Comparison of numerical and experimental results, Appl. Surf. Sci. 257 (2011) 5465–5469. doi:10.1016/j.apsusc.2010.11.157.
[17] H. Yang, H. He, L. Zhou, J. Qian, J. Hao, H. Zhu, Sharp transition of laser-induced periodic ripple structures, Opt. Appl. 42 (2012) 795–803.
[18] F. Fraggelakis, G. Mincuzzi, J. Lopez, I. Manek-Hönninger, R. Kling, Texturing metal surface with MHz ultra-short laser pulses, Opt. Express. 25 (2017) 18131. doi:10.1364/OE.25.018131.
[19] F. Bauer, A. Michalowski, T. Kiedrowski, S. Nolte, Heat accumulation in ultra-short pulsed scanning laser ablation of metals, Opt. Express. 23 (2015) 1035–1043. doi:10.1364/OE.23.001035.
[20] X. Ji, L. Jiang, X. Li, W. Han, Y. Liu, A. Wang, Y. Lu, Femtosecond laser-induced cross-periodic structures on a crystalline silicon surface under low pulse number irradiation, Appl. Surf. Sci. 326 (2015) 216–221. doi:10.1016/j.apsusc.2014.11.124.
[21] N. Tsutsumi, A. Fujihara, K. Nagata, Fabrication of laser induced periodic surface structure for geometrical engineering, Thin Solid Films. 517 (2008) 1487–1492. doi:10.1016/j.tsf.2008.09.025.
[22] E. Skoulas, A. Manousaki, C. Fotakis, E. Stratakis, Biomimetic surface structuring using cylindrical vector femtosecond laser beams, Sci. Rep. 7 (2017) srep45114. doi:10.1038/srep45114.
[23] M.H. Dar, N.A. Saad, C. Sahoo, S.R.G. Naraharisetty, N.R. Desai, Ultrafast laser-induced reproducible nano-gratings on a molybdenum surface, Laser Phys. Lett. 14 (2017) 026101. doi:10.1088/1612-202X/aa5129.
[24] P. Gregorčič, M. Sedlaček, B. Podgornik, J. Reif, Formation of laser-induced periodic surface structures (LIPSS) on tool steel by multiple picosecond laser pulses of different polarizations, Appl. Surf. Sci. 387 (2016) 698–706. doi:10.1016/j.apsusc.2016.06.174.
[25] J. Reif, C. Martens, S. Uhlig, M. Ratzke, O. Varlamova, S. Valette, S. Benayoun, On large area LIPSS coverage by multiple pulses, Appl. Surf. Sci. 336 (2015) 249–254. doi:10.1016/j.apsusc.2014.11.153.
[26] J. Lehr, A.-M. Kietzig, Production of homogenous micro-structures by femtosecond laser micro-machining, Opt. Lasers Eng. 57 (2014) 121–129. doi:10.1016/j.optlaseng.2014.01.012.
[27] L. Gemini, M. Faucon, L. Romoli, R. Kling, High throughput laser texturing of super-hydrophobic surfaces on steel, in: Proc SPIE 10092, 2017: p. 100921G–100921G–6. doi:10.1117/12.2252649.
[28] M. Ardron, N. Weston, D. Hand, A practical technique for the generation of highly uniform LIPSS, Appl. Surf. Sci. 313 (2014) 123–131. doi:10.1016/j.apsusc.2014.05.154.
[29] A.R. de la Cruz, R. Lahoz, J. Siegel, G.F. de la Fuente, J. Solis, High speed inscription of uniform, large-area laser-induced periodic surface structures in Cr films using a high repetition rate fs laser, Opt. Lett. 39 (2014) 2491–2494. doi:10.1364/OL.39.002491.
[30] G. Mincuzzi, L. Gemini, M. Faucon, R. Kling, Extending ultra-short pulse laser texturing over large area, Appl. Surf. Sci. 386 (2016) 65–71. doi:10.1016/j.apsusc.2016.05.172.

[31] F. Preusch, S. Rung, R. Hellmann, Influence of Polishing Orientation on the Generation of LIPSS on Stainless Steel, J. Laser Micro Nanoeng. 11 (2016) 137–142. doi:10.2961/jlmn.2016.01.0025.
[32] G.R.B.E. Römer, A.J. Huis in't Veld, J. Meijer, M.N.W. Groenendijk, On the formation of laser induced self-organizing nanostructures, CIRP Ann. - Manuf. Technol. 58 (2009) 201–204. doi:10.1016/j.cirp.2009.03.068.
[33] M. Huang, F. Zhao, Y. Cheng, N. Xu, Z. Xu, Origin of Laser-Induced Near-Subwavelength Ripples: Interference between Surface Plasmons and Incident Laser, ACS Nano. 3 (2009) 4062–4070. doi:10.1021/nn900654v.
[34] J.T. Cardoso, A. Garcia-Girón, J.M. Romano, D. Huerta-Murillo, R. Jagdheesh, M. Walker, S.S. Dimov, J.L. Ocaña, Influence of ambient conditions on the evolution of wettability properties of an IR-, ns-laser textured aluminium alloy, RSC Adv. 7 (2017) 39617–39627. doi:10.1039/C7RA07421B.
[35] B. Tan, K. Venkatakrishnan, A femtosecond laser-induced periodical surface structure on crystalline silicon, J. Micromechanics Microengineering. 16 (2006) 1080. doi:10.1088/0960-1317/16/5/029.
[36] M. Barberoglou, D. Gray, E. Magoulakis, C. Fotakis, P.A. Loukakos, E. Stratakis, Controlling ripples' periodicity using temporally delayed femtosecond laser double pulses, Opt. Express. 21 (2013) 18501–18508. doi:10.1364/OE.21.018501.
[37] J.F. Young, J.S. Preston, H.M. van Driel, J.E. Sipe, Laser-induced periodic surface structure. II. Experiments on Ge, Si, Al, and brass, Phys. Rev. B. 27 (1983) 1155–1172. doi:10.1103/PhysRevB.27.1155.
[38] J. Bonse, A. Rosenfeld, J. Krüger, On the role of surface plasmon polaritons in the formation of laser-induced periodic surface structures upon irradiation of silicon by femtosecond-laser pulses, J. Appl. Phys. 106 (2009) 104910. doi:10.1063/1.3261734.
[39] G. Baraldi, S. Bakhti, Z. Liu, S. Reynaud, Y. Lefkir, F. Vocanson, N. Destouches, Polarization-driven self-organization of silver nanoparticles in 1D and 2D subwavelength gratings for plasmonic photocatalysis, Nanotechnology. 28 (2017) 035302. doi:10.1088/1361-6528/28/3/035302.
[40] S. Hou, Y. Huo, P. Xiong, Y. Zhang, S. Zhang, T. Jia, Z. Sun, J. Qiu, Z. Xu, Formation of long- and short-periodic nanoripples on stainless steel irradiated by femtosecond laser pulses, J. Phys. Appl. Phys. 44 (2011) 505401. doi:10.1088/0022-3727/44/50/505401.
[41] O. Varlamova, F. Costache, M. Ratzke, J. Reif, Control parameters in pattern formation upon femtosecond laser ablation, Appl. Surf. Sci. 253 (2007) 7932–7936. doi:10.1016/j.apsusc.2007.02.067.
[42] A.-M. Kietzig, S.G. Hatzikiriakos, P. Englezos, Patterned Superhydrophobic Metallic Surfaces, Langmuir. 25 (2009) 4821–4827. doi:10.1021/la8037582.
[43] Y. Zhang, G. Zou, L. Liu, Y. Zhao, Q. Liang, A. Wu, Y.N. Zhou, Time-dependent wettability of nano-patterned surfaces fabricated by femtosecond laser with high efficiency, Appl. Surf. Sci. 389 (2016) 554–559. doi:10.1016/j.apsusc.2016.07.089.
[44] N. Yasumaru, E. Sentoku, J. Kiuchi, Formation of organic layer on femtosecond laser-induced periodic surface structures, Appl. Surf. Sci. 405 (2017) 267–272. doi:10.1016/j.apsusc.2017.02.084.
[45] A. Cunha, A.P. Serro, V. Oliveira, A. Almeida, R. Vilar, M.-C. Durrieu, Wetting behaviour of femtosecond laser textured Ti–6Al–4V surfaces, Appl. Surf. Sci. 265 (2013) 688–696. doi:10.1016/j.apsusc.2012.11.085.